https://doi.org/10.5194/egusphere-2026-6435
Preprint. Discussion started: 26 October 2026
© Author(s) 2026. CC BY 4.0 License.

Wind-driven forest seismicity encodes tree water status

Josefine Umlauft[1], Karin Mora[2], Fabian Limberger[3], Kilian Gerberding[4], Stefanie Dumberger[5], Simon Haberstroh[5], Markus Sulzer[6], Lea Dedden[7], Markus Weiler[7], Christian Wirth[8], Christiane Werner[5], and Teja Kattenborn[4]

[1]ScaDS.AI - Center for Scalable Data Analytics and Artificial Intelligence, Leipzig University, Saxony, Germany
[2]Institute for Earth System Science & Remote Sensing, Leipzig University, Saxony, Germany
[3]Goethe University Frankfurt am Main, Hessen, Germany
[4]Sensor-based Geoinformatics, Faculty of Environment and Natural Resources, University of Freiburg, Baden-Württemberg, Germany
[5]Ecosystem Physiology, Faculty of Environment and Natural Resources, University of Freiburg, Baden-Württemberg, Germany
[6]Environmental Meteorology, Faculty of Environment and Natural Resources, University of Freiburg, Baden-Württemberg, Germany
[7]Hydrology, Faculty of Environment and Natural Resources, University of Freiburg, Baden-Württemberg, Germany
[8]Institute of Systematic Botany and Functional Biodiversity, Leipzig University, Saxony, Germany

Correspondence: Josefine Umlauft (josefine.umlauft@uni-leipzig.de)

Abstract. Wind-driven tree motion generates ground vibrations that can be recorded by seismic sensors. While wind provides the excitation, the resulting motion may also reflect the condition of the trees. We test whether seismic observations contain information on tree water status beyond that provided by meteorological and soil moisture measurements. We combine observations from three growing seasons (2024–2026) at the ECOSENSE forest in southwestern Germany: five broadband seismometers, meteorological and soil moisture measurements, and high-resolution stem-diameter measurements from four mature Douglas firs (*Pseudotsuga menziesii*) and four mature European beeches (*Fagus sylvatica*). From the stem-diameter records, we derive tree water deficit (TWD), which quantifies reversible stem shrinkage and serves as an indicator of tree water status. We use principal component analysis to characterize collective seismic dynamics and gradient-boosted tree models to test whether seismic observations improve TWD prediction beyond environmental predictors. The seismic network forms a continuous, structured latent space organized by wind. For the illustrated tree, TWD does not define a separate seismic regime but is associated with differences in how observations populate this latent space. Adding seismic predictors improves held-out TWD prediction for many tree–station combinations, both with and without soil moisture in the baseline, but gains vary substantially among trees and stations. For Douglas fir Pm1 and station C6A, adding seismic predictors to meteorology and soil moisture increases held-out R^2 from 0.64 to 0.80 and reduces RMSE by 26.4%. Other combinations show smaller gains or deterioration. These findings indicate that the seismic response of a wind-driven forest contains information associated with tree water status beyond the measured environmental conditions. Ground-based seismic sensing could therefore complement direct physiological measurements in multimodal forest monitoring.

https://doi.org/10.5194/egusphere-2026-6435
Preprint. Discussion started: 26 October 2026
© Author(s) 2026. CC BY 4.0 License.

1 Introduction

Increasing exposure to drought and heat threatens forest functioning and persistence (Allen et al., 2015; Werner et al., 2025; Gessler et al., 2026). Understanding how trees respond to changing atmospheric and hydrological conditions requires observations that capture physiological dynamics over extended periods and across multiple locations. Measurements on individual trees provide detailed information, while complementary approaches can help place those responses in the context of broader forest dynamics (Mahecha et al., 2024).

Tree water status and hydraulic responses can be characterized, for example, using measurements of sap flow, water potential, and stem diameter variation (Dietrich et al., 2018; Haberstroh et al., 2025; Peters et al., 2025; Dumberger et al., 2025). Continuous dendrometer measurements resolve changes in stem diameter associated with growth and variation in tree water storage. Tree water deficit (TWD) describes the reversible stem shrinkage relative to a reference diameter and reflects changes in internal water storage (Zweifel et al., 2005; Hackmann et al., 2024). It is related to other indicators of tree water status, including water potential (Ziegler et al., 2024; Peters et al., 2025; Magh et al., 2026) and sap flow (Brinkmann et al., 2016; Donfack et al., 2026). TWD varies diurnally as stems shrink during daytime water use and recover overnight. A larger instantaneous TWD therefore does not necessarily indicate physiological stress, because the extent of reversible shrinkage also depends on species- and tree-specific water-use strategies (Dietrich et al., 2018; Peters et al., 2025). In contrast, increasing daily minimum TWD ($\mathrm{TWD}_{\mathrm{min}}$) indicates incomplete overnight replenishment of stem water reserves and can signal persistent water deficits and increased physiological stress (Zweifel et al., 2020). TWD and other physiological indicators can vary even among individuals of the same species. Measurements therefore characterize the monitored trees, and extrapolation to broader forest water status requires accounting for this variability.

Tree motion may provide a complementary view of these dynamics. Trees move in response to wind, with the resulting motion shaped by architecture, mass distribution, stiffness, and damping (Moore and Maguire, 2004; Jackson et al., 2019). Changes in water storage could modify this mechanical response. Accelerometer studies have reported variation in tree sway associated with water status and canopy water storage (Ciruzzi and Loheide II, 2019, 2021; van Emmerik et al., 2017). Such associations must be considered within the much stronger influence of wind forcing.

Wind-driven tree motion also generates ground vibrations through the root–soil system (Johnson et al., 2019). At the ECOSENSE forest, we previously showed that ground-based seismometers record dominant sway frequencies corresponding to those measured by trunk-mounted accelerometers, and that seismic spectra change systematically with wind forcing (Umlauft et al., 2025). These findings established wind-driven tree sway as a source of low-frequency ground vibrations at this site and demonstrated the potential to infer wind conditions from seismic observations. However, that study did not examine whether these seismic signals also carry information about tree water status.

Ground-based seismic sensors can thus monitor aspects of tree dynamics without attachment to individual trees. Because each station may receive vibrations from several sources, a distributed network records a spatially heterogeneous response rather than the motion of a uniquely associated tree.

https://doi.org/10.5194/egusphere-2026-6435
Preprint. Discussion started: 26 October 2026
© Author(s) 2026. CC BY 4.0 License.

Whether this response also carries information about tree water status remains unresolved. Detecting such information requires distinguishing water-status-related variation from the strong influence of wind forcing. Moreover, soil conditions may affect both tree water status (Brinkmann et al., 2016) and seismic wave propagation, as changes in soil water content can alter near-surface seismic velocities (Shen et al., 2024). These shared environmental influences need to be considered when interpreting associations between seismic observations and TWD.

Here, we analyse three growing seasons at the ECOSENSE forest: 5 July–30 September 2024, 1 May–30 September 2025, and 1 May–30 August 2026 (Werner et al., 2024; Tesch et al., 2025). Five seismic stations sample ground motion across an approximately 400 m^2 forest plot. We combine their observations with meteorological data, soil moisture from one local profile, and dendrometer-derived TWD from eight trees within and around the plot: four Douglas firs and four European beeches. We first examine how wind organizes the seismic network response and whether TWD is associated with variation within the network. We then compare TWD predictions for individual tree–station combinations to determine whether seismic features add information beyond meteorological predictors, both with and without soil moisture included in the baseline.

2 Methods

2.1 Study site and observational data

The study was conducted at the ECOSENSE experimental forest near Ettenheim in southwestern Germany, at the foothills of the Black Forest (Werner et al., 2024) (Fig. 1A). ECOSENSE is an interdisciplinary forest-observation platform combining measurements of atmospheric, vegetation, and soil processes (Tesch et al., 2026). The present study focuses on an approximately 400 m^2 plot within this platform. Point dendrometers measure stem diameter changes on individual trees, five seismometers record ground vibrations at different locations within the plot, and atmospheric forcing is characterized using measurements from the nearby meteorological tower. The eight dendrometer-equipped trees are located within and immediately around the seismic plot (Fig. 1A). The measurement design is spatially distributed rather than based on one-to-one tree–station pairs: each dendrometer records an individual tree, whereas each seismic station samples a ground-vibration field influenced by multiple surrounding trees.

The forest is structurally heterogeneous and dominated by European beech (*Fagus sylvatica*) and Douglas fir (*Pseudotsuga menziesii*), with additional Norway spruce (*Picea abies*), pedunculate oak (*Quercus robur*), silver fir (*Abies alba*), and Scots pine (*Pinus sylvestris*). Trees of different ages and dimensions occur in mixed and monospecific patches, resulting in a heterogeneous stand structure. European beeches are approximately 55–110 years old, 24–28 m tall and have a diameter at breast height (DBH) of 37.1 ± 7.1 cm, whereas Douglas firs are younger (45–50 years) and approximately 27–30 m tall with a DBH of 49.5 ± 14.3 cm (Dumberger et al., 2026).

In July 2024, the ECOSENSE infrastructure was complemented by a seismic network for long-term, quasi-continuous monitoring of ground vibrations within the forest plot (Fig. 1A,B). The network, which was used in the previous study to establish wind-driven tree sway (Umlauft et al., 2025), comprises five three-component broadband seismometers (Trillium Compact 120 s, Nanometrics; stations C66, C67, C68, C69, and C6A) connected to DATA-CUBE3 recorders (DIGOS/Omnirecs). The

https://doi.org/10.5194/egusphere-2026-6435
Preprint. Discussion started: 26 October 2026
© Author(s) 2026. CC BY 4.0 License.

stations are distributed across the same structurally heterogeneous stand and sample spatial variability in its ground-vibration field. Ground velocity is recorded continuously at 100 Hz. To improve ground coupling and reduce direct environmental disturbance, the sensors were installed approximately 30 cm below the surface on concrete slabs (Fig. 1B).

Station locations were constrained by the existing multisensor infrastructure and dense forest structure rather than by fixed distances to individual tree stems. Consequently, individual seismic stations do not represent dedicated measurements of single trees but record ground motion generated by multiple surrounding vegetation sources. The seismic network is therefore treated as a spatially distributed observation of the forest vibration field.

Custom-made point dendrometers based on potentiometers (Model 9605 BEI, Duncan Electronics, Commerce, Texas, USA), following Dumberger et al. (2026), were installed at 1.30 m stem height on eight trees (Fig. 1A,C). Sensors were mounted on metal angle brackets fixed to the trunk with two stainless-steel rods. For Douglas firs, the bark was gently removed at the sensor location before installation to exclude the swelling and shrinking effects of the bark. Stem diameter variations were recorded at 15-min intervals using CR1000 data loggers (Campbell Scientific Ltd., Shepshed, UK). Tree water deficit (TWD) was derived using the *treenetprock* package (Knüsel et al., 2021) and the zero-growth approach introduced by Zweifel et al. (2016). In this approach, TWD represents reversible stem shrinkage relative to a growth-based reference diameter, separating it from irreversible stem growth.

The monitored trees comprise four Douglas firs (Pm1, Pm2, Pm4, and Pm5) and four European beeches (Fm1, Fm2, Fm4, and Fm5), located within and around the seismic plot (Fig. 1A). These individuals span different positions relative to the seismic stations and constitute the trees for which TWD is analysed in this study. TWD observations for Fm1 in 2024 and parts of 2026 were excluded due to sensor failure.

Meteorological conditions were recorded at the nearby meteorological tower (Fig. 1A). Wind speed and gusts were measured using a wind monitor (Young 05103, R. M. Young Company, Traverse City, MI, USA), while precipitation was measured using an infrared forward-scatter visibility and present-weather sensor (CS125, Campbell Scientific Inc., Shepshed, UK), both installed near the top of the tower. Air temperature and relative humidity were measured at 2 and 46 m using digital sensors housed in passively ventilated radiation shields (HygroVue 10 and RAD10E, Campbell Scientific Inc., Shepshed, UK).

Soil moisture was recorded along a soil moisture profile within the study plot (Fig. 1A). Measurements at 0.3, 0.5, 0.7, and 0.9 m depth were used to characterize local soil moisture conditions. Soil moisture was measured at 15-min intervals with one sensor at each depth (SMT100, Truebner GmbH, Neustadt, Germany), operating on the Time-Domain Transmissometry (TDT) principle. Soil moisture was used as the sensor-calculated volumetric water content [vol. %], based on the soil dielectric permittivity, using the Topp equation (Topp et al., 1980). All soil moisture measurements were quality controlled following the Dorigo et al. (2013) scheme adapted to the site conditions.

The analyses focus on three growing-season periods: 5 July–30 September 2024, 1 May–30 September 2025, and 1 May–30 August 2026 (Fig. 1D). The intervening winter periods are excluded from the analyses, including to avoid cold-temperature effects on stem diameter variations. In addition to these seasonal gaps, the seismic records contain irregular, station-dependent data gaps, primarily due to battery depletion and occasional instrument failures.

https://doi.org/10.5194/egusphere-2026-6435
Preprint. Discussion started: 26 October 2026
© Author(s) 2026. CC BY 4.0 License.

Meteorological, soil moisture, physiological, and derived seismic observations are aligned on a common 15-min temporal grid for the corresponding analyses. The resulting dataset captures temporal variability in meteorological forcing, soil moisture, seismic spectral characteristics, and TWD across the three growing seasons (Fig. 1D). Season-aggregated data coverage and the temporal distribution of data gaps are summarized in Table S1 and Fig. S1, respectively.

2.2 Seismic preprocessing and feature extraction

Previous simultaneous measurements with tree-mounted accelerometers and ground-based seismometers at this site identified corresponding, tree-specific sway frequencies in both datasets (Umlauft et al., 2025). These results provide the observational basis for interpreting the low-frequency ground vibrations analysed here as being predominantly generated by wind-induced tree motion. Because wind-induced tree sway is primarily horizontal, and the relationship between tree acceleration and ground motion was previously established using horizontal motion, the present analysis focuses on the two horizontal seismic components. The vertical component may contain complementary information but is not considered here.

Continuous seismic records are processed independently for each of the five stations, with the two horizontal components (E–W and N–S) retained separately throughout time-domain preprocessing. The records are divided into overlapping two-day blocks with a one-day step, allowing blockwise processing with temporal buffers around the retained data. To minimize filter-edge effects, the outer 6 h of each block are discarded. The retained segments are then combined into continuous, component-specific time series, averaging valid values where segments overlap.

Within each contiguous finite-data segment, the signal mean is removed and the data are bandpass filtered between 0.1 and 1.0 Hz to focus on the low-frequency ground motion associated with tree sway (Umlauft et al., 2025). A fourth-order Butterworth filter is applied forwards and backwards to obtain zero-phase filtering. Processing finite-data segments separately preserves data gaps during filtering. The filtered signals are subsequently downsampled onto a common 5-Hz time grid, reducing data volume while retaining the analysed frequency band below the Nyquist frequency of 2.5 Hz. Blocks containing inconsistent sampling rates within or between components, or sampling rates incompatible with integer downsampling to 5 Hz, are excluded.

Two complementary sets of seismic descriptors are derived from the processed horizontal components. First, general statistical and spectral features are calculated in non-overlapping 15-min windows, matching the temporal resolution of the TWD measurements. Data gaps, caused primarily by battery depletion and occasional instrument downtime, generally affect the complete station record. Because the two horizontal components are processed independently, only samples that are valid in both components are used for feature extraction. Time-domain variance is calculated separately for both components and represented by their mean, whereas skewness and excess kurtosis are retained separately for each component.

Spectral features are estimated only for windows with at least 95% joint data coverage, balancing data retention against the influence of missing samples. Within retained windows, samples that are invalid in either component are removed, and the remaining jointly valid samples are concatenated for spectral estimation. Power spectral densities (PSDs) are estimated separately for the E–W and N–S components using Welch's method (Welch, 1967) with a Hann window, 120-s segments, and 50% overlap. The segment duration balances frequency detail (nominal frequency spacing of approximately 0.0083 Hz) against

https://doi.org/10.5194/egusphere-2026-6435
Preprint. Discussion started: 26 October 2026
© Author(s) 2026. CC BY 4.0 License.

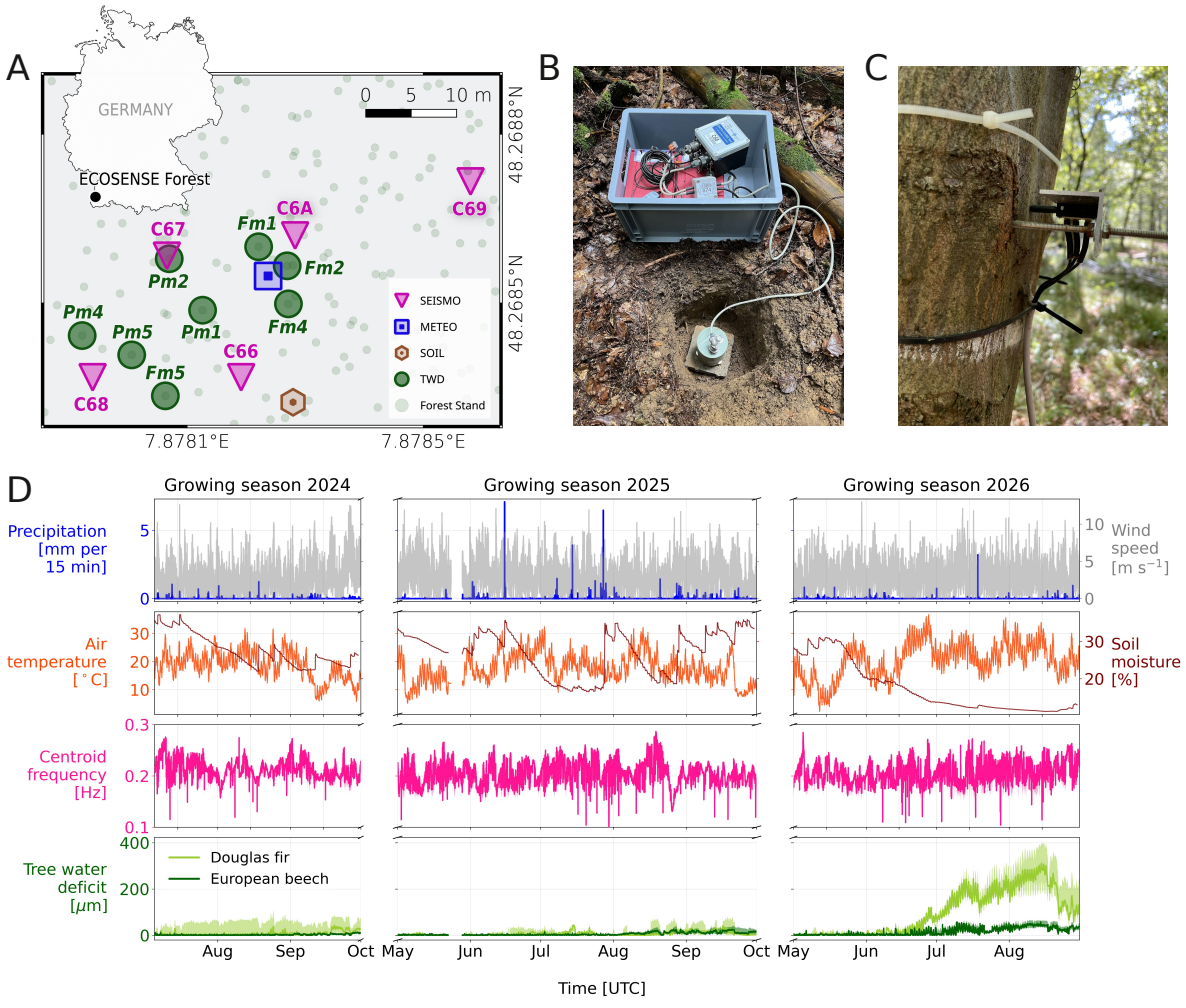


Figure 1. Study site, measurement setup, and observational dataset. **(A)** Location and spatial configuration of the ECOSENSE forest monitoring site in southwestern Germany. The black dot in the Germany overview marks the site location. In the detailed map, small pale-green circles indicate mapped trees, large dark-green outlined circles indicate dendrometer-equipped trees (TWD), inverted pink triangles indicate seismic stations (SEISMO), the blue square indicates the meteorological tower (METEO), and the brown hexagon indicates the soil moisture profile (SOIL). **(B)** Example of the seismic installation before burial, showing a broadband three-component seismometer connected to a DATA-CUBE3 recorder. The same setup was used at stations C66, C67, C68, C69, and C6A. **(C)** Example of a point dendrometer used to derive tree water deficit (TWD). Dendrometers were installed on four Douglas firs (Pm1, Pm2, Pm4, and Pm5) and four European beeches (Fm1, Fm2, Fm4, and Fm5). **(D)** Observations on a common 15-min grid during the 2024, 2025, and 2026 growing seasons. From top to bottom: precipitation (blue) and wind speed at 47 m (grey); air temperature at 2 m (orange) and soil moisture (brown; median across depths of 0.3, 0.5, 0.7, and 0.9 m); seismic spectral centroid frequency (pink); and TWD for Douglas fir (light green) and European beech (dark green). For centroid frequency and TWD, lines show medians and shading indicates the 20th–80th percentile range across seismic stations and across trees within each species, respectively. Breaks in the time axis separate the growing seasons. Times are given in UTC.

https://doi.org/10.5194/egusphere-2026-6435
Preprint. Discussion started: 26 October 2026
© Author(s) 2026. CC BY 4.0 License.

the number of segments available for averaging within each 15-min window. The Hann taper reduces spectral leakage, while 50% overlap provides a conventional compromise between effective use of the tapered data and redundancy between adjacent segments. The component PSDs are subsequently combined to obtain the mean horizontal power spectrum,

$$P_{\mathrm{H}}(f) = \frac{P_{\mathrm{E--W}}(f) + P_{\mathrm{N--S}}(f)}{2}. \tag{1}$$

All spectral descriptors are derived from this mean horizontal PSD. These comprise the frequency and power of the dominant spectral peak within 0.1–1.0 Hz, as well as integrated spectral power within the frequency bands 0.10–0.20, 0.10–0.30, 0.20–0.50, and 0.50–1.00 Hz. These bands summarize the distribution of power across the analysed interval; the overlapping 0.10–0.30 Hz band additionally captures broader low-frequency power spanning the narrower band boundaries.

To characterize slowly varying frequency dynamics of the forest vibration field, we additionally derive a spectral track using overlapping 1-h windows, with consecutive windows starting 15 min apart. The longer windows provide finer frequency detail than the 120-s segments used for the 15-min features, while the 15-min step provides a sampling interval consistent with the TWD measurements. Consecutive hourly estimates share data and are therefore temporally dependent. All feature windows are timestamped at their centres.

For each component and 1-h window, the PSD is calculated from a single Hann-tapered segment spanning the full hour, using an FFT length of 131072 samples. Zero-padding provides a densely sampled frequency grid for peak interpolation without increasing the underlying spectral resolution, which is governed by the segment duration and taper. Only windows with complete joint valid data coverage are retained. The component PSDs are averaged to obtain the mean horizontal PSD, and spectral characteristics are evaluated within 0.10–0.35 Hz, focusing on the low-frequency portion of the analysed spectrum while remaining within the preprocessing passband.

Two frequency descriptors are derived from the mean horizontal PSD: the dominant frequency, defined by the maximum PSD amplitude within this interval and refined using sub-bin quadratic peak interpolation, and the spectral centroid frequency,

$$f_{\mathrm{centroid}} = \frac{\sum_i f_i P_{\mathrm{H}}(f_i)}{\sum_i P_{\mathrm{H}}(f_i)}, \tag{2}$$

where the sums extend over frequency bins within 0.10–0.35 Hz and $P_{\mathrm{H}}(f_i)$ denotes the mean horizontal spectral power at frequency f_i. The spectral centroid summarizes the distribution of power across the selected interval rather than relying on a single spectral peak. It is used as the primary seismic descriptor for the network latent-space analysis following an exploratory comparison in which it provided the clearest network organization among the tested frequency descriptors.

2.3 Tree water deficit, meteorological, and soil moisture data

TWD is used as the target variable representing tree water status. The dendrometer measurements and derived TWD series are available at 15-min intervals and define the temporal resolution of the common analysis grid, with a separate TWD series retained for each monitored tree.

https://doi.org/10.5194/egusphere-2026-6435
Preprint. Discussion started: 26 October 2026
© Author(s) 2026. CC BY 4.0 License.

Meteorological observations are aggregated to 15-min intervals. Precipitation depth is obtained by integrating the one-minute CS125 precipitation rates over each interval and is expressed in mm. Because the source sampling interval is one minute, this is numerically equivalent to summing the recorded values. Missing readings are omitted, so partially observed intervals represent only the recorded rainfall; intervals without valid readings remain missing. Air temperature and relative humidity are averaged. Wind predictors comprise the mean, maximum, and standard deviation of the recorded wind-speed series within each 15-min interval, together with the interval means of wind direction and of the separately recorded maximum-wind-speed series.

Soil moisture measurements from one profile within the study plot were summarized as the median across the available measurements at 0.3, 0.5, 0.7, and 0.9 m depth. The resulting series was aggregated to the common 15-min grid using the median within each interval.

For analyses that distinguish physiological states, wet and dry conditions are defined separately for each tree based on its TWD distribution. Observations at or below the 20th percentile are classified as wet and observations at or above the 80th percentile as dry. Intermediate observations are retained for analyses using continuous TWD but excluded from explicit comparisons between wet and dry states.

2.4 Seismic network latent-space analysis

We use principal component analysis (PCA) to characterize the collective dynamics of the five-station seismic network. The primary latent-space representation is constructed from the spectral centroid frequency derived independently at each station from the spectral analysis described above. Each centroid estimate represents a 1-h seismic window, with consecutive windows starting 15 min apart, yielding a time-resolved description of the frequency distribution of the forest vibration field at 15-min intervals.

For each seismic descriptor, observations from stations C66, C67, C68, C69, and C6A within the three growing seasons are assembled into a matrix in which columns correspond to stations and rows to observation times. Timestamps with data from fewer than two seismic stations are excluded. To emphasize relative spatial variation across the network rather than variations common to all stations, the instantaneous network-wide mean is subtracted from the available station values at each timestamp. Remaining station-specific data gaps are filled with the median of the corresponding station time series, after which each station is standardized to zero mean and unit variance before PCA. This procedure allows the latent-space analysis to retain periods with partial network coverage.

PCA is fitted independently for each seismic descriptor. Up to five components are calculated from the five stations. Subtracting the instantaneous network mean removes the common-mode variation and would constrain a complete-data representation to at most four independent dimensions. With partial network coverage, subsequent station-wise median imputation need not preserve this constraint, so a small fifth component can remain. The first four components are examined in the latent-space analyses, with occupancy calculated in PC1–PC2. Station loadings are examined to quantify the contribution of individual stations to each component.

The influence of meteorological forcing on the seismic latent space is examined by projecting wind speed onto the PCA scores, restricted to timestamps with corresponding meteorological observations. For stratified analyses, observations are sep-

https://doi.org/10.5194/egusphere-2026-6435
Preprint. Discussion started: 26 October 2026
© Author(s) 2026. CC BY 4.0 License.

arated into three wind-speed classes: low wind (< 2 m s^{-1}), moderate wind (2–5 m s^{-1}), and high wind (> 5 m s^{-1}). These thresholds distinguish the predominant low-to-moderate wind conditions from less frequent high-wind conditions while retaining sufficient observations in each class (Fig. S2).

Associations between the seismic latent space and tree water status are evaluated separately for each tree and restricted to timestamps for which TWD observations for the respective tree are available. This tree-specific treatment accounts for differences in TWD data availability among the monitored individuals.

2.4.1 Physiological occupancy of the seismic latent space

To examine whether tree water status is associated with the collective seismic response, TWD observations are mapped onto the seismic PCA latent space at corresponding timestamps. Analyses are performed separately for each tree and restricted to timestamps with available TWD observations. Wet and dry conditions, defined by the tree-specific 20th and 80th percentiles of the TWD distribution, are then compared within the PC1–PC2 latent space.

To assess whether relevant structure extends beyond the dominant PC1–PC2 plane, we additionally examine pairwise projections involving PC3 and PC4. Their organization is evaluated with respect to station contributions, TWD, wind speed, and growing season.

The quantitative occupancy analysis is performed in the PC1–PC2 latent space, which is discretized into a 45×45 grid. For each occupied bin, the numbers of wet and dry observations are determined and used to estimate the conditional probability of dry conditions among the wet and dry observations in each seismic-state bin. Bins containing fewer than 10 observations are excluded from the conditional-probability analysis. Conditional occupancy is evaluated both across all wind conditions and separately within the three wind-speed classes defined above to assess whether associations with tree water status persist under comparable wind forcing.

2.4.2 Robustness across seismic features

To determine whether the network organization identified from spectral centroid frequency is robust to the choice of seismic descriptor, the PCA workflow is repeated independently for excess kurtosis, peak PSD frequency, variance, dominant PSD peak power, and bandpower in the 0.10–0.20, 0.10–0.30, 0.20–0.50, and 0.50–1.00 Hz frequency bands.

Because independently fitted PCA solutions can differ in component ordering and sign, candidate components are aligned to the centroid-frequency reference solution by identifying the component with the maximum absolute correlation between PC-score time series. The sign of the matched component is adjusted where necessary before the correspondence between latent-space representations is evaluated. This allows similarities among seismic descriptors to be assessed independently of arbitrary PCA sign and component-order ambiguities.

https://doi.org/10.5194/egusphere-2026-6435
Preprint. Discussion started: 26 October 2026
© Author(s) 2026. CC BY 4.0 License.

2.5 Machine learning prediction of tree water deficit

We use gradient-boosted decision trees to test whether seismic observations contain predictive information on TWD beyond that available from meteorological forcing and, in a separate comparison, soil moisture. Models are implemented using XGBoost (Chen and Guestrin, 2016) and evaluated separately for individual tree–station combinations. Candidate models are generated for the eight monitored trees and five seismic stations; combinations without sufficient joint observations are excluded from analysis.

For each tree–station combination, the target variable is the TWD of the respective tree. Meteorological predictors comprise the five wind summaries described above, precipitation depth, mean air temperature at 2 and 46 m, and mean relative humidity at 2 and 46 m. Soil moisture enters only the soil-adjusted model configurations. Seismic predictors are restricted to features from the respective seismic station and comprise seismic summary descriptors and bandpower features.

For each tree–station combination, observations missing TWD or any of the selected meteorological, soil-moisture, or seismic predictors are excluded before splitting the data. All four primary models (METEO, METEO + SOIL, METEO + SEISMO, and METEO + SOIL + SEISMO) are therefore trained and tested on identical timestamps within that pair. This matched-sample design prevents differences in coverage from being mistaken for the added predictive value of seismic features.

2.5.1 Temporal train–test splitting

To reduce temporal dependence between training and test data, we use blocked rather than randomly sampled train–test partitions. Predictive analyses are restricted to the three growing seasons defined above. Block construction is performed separately within each growing season so that temporal blocks do not span the intervening seasonal gaps.

Each growing season is divided into consecutive 120-h blocks. Even-numbered blocks are assigned to the training dataset and odd-numbered blocks to the test dataset. Thus, training and test observations alternate through time while remaining grouped into five-day intervals. The same temporal block assignment is used for all model variants within each tree–station combination. This blocked evaluation assesses generalization to unseen multi-day periods within the observed growing seasons; it does not test transfer to an entirely unseen growing season.

2.5.2 Model configurations and evaluation

Six model configurations are evaluated. METEO predicts TWD using meteorological variables alone, and SEISMO uses only features from the respective seismic station. METEO + SEISMO combines the two predictor sets. METEO + SOIL adds soil moisture to the meteorological predictors, while METEO + SOIL + SEISMO additionally includes the station-specific seismic features. Finally, the residual-correction model uses a seismic model to predict residual variation left by METEO + SOIL.

For the residual-correction model, METEO + SOIL is first fitted to TWD. Within the training data, out-of-fold baseline predictions are generated by block-based cross-validation, and residuals are calculated as the difference between observed and predicted TWD. A second XGBoost model is trained to predict these residuals using only seismic predictors from the respective

https://doi.org/10.5194/egusphere-2026-6435
Preprint. Discussion started: 26 October 2026
© Author(s) 2026. CC BY 4.0 License.

station. For the held-out test data, the predicted seismic residual correction is added to the METEO + SOIL prediction to obtain the final residual-corrected estimate.

XGBoost hyperparameters are optimized independently for each tree–station combination and each fitted model configuration using only the corresponding training data. Hyperparameter selection uses group-based cross-validation, with the 120-h temporal blocks as groups so that observations from the same block are never divided between training and validation subsets. Five folds are used where the number of available training blocks permits. Held-out test blocks are not used during hyperparameter selection.

Preliminary tests conducted exclusively on training data explored a broader range of settings. The final grid comprises 48 parameter combinations: 100 or 200 trees; maximum tree depths of 3, 4, or 6; learning rates of 0.03 or 0.05; and row and feature subsampling fractions of 0.8 or 1.0. The parameter combination minimizing the cross-validated mean squared error is refitted using the complete training dataset and evaluated on the unchanged held-out test data. For the residual-correction model, the L1 and L2 regularization parameters are fixed at 0.5 and 1.5, respectively. Selected hyperparameters and their cross-validation scores are retained for each fitted model.

Model performance is quantified using the coefficient of determination (R^2), Pearson correlation coefficient (CC), root-mean-square error (RMSE), and mean absolute error (MAE). Held-out test performance provides the primary evaluation. The added predictive value of seismic information beyond meteorology is quantified as

$$\Delta R^2_{\mathrm{METEO}} = R^2_{\mathrm{METEO+SEISMO}} - R^2_{\mathrm{METEO}}. \tag{3}$$

Its added value beyond meteorology and soil moisture is quantified separately as

$$\Delta R^2_{\mathrm{METEO+SOIL}} = R^2_{\mathrm{METEO+SOIL+SEISMO}} - R^2_{\mathrm{METEO+SOIL}}. \tag{4}$$

Both differences are calculated on the corresponding matched held-out test observations. The difference between the residual-corrected model and METEO + SOIL is assessed as an additional formulation of the soil-adjusted comparison.

Relative RMSE reduction is calculated for each matched baseline comparison as

$$G_{\mathrm{RMSE}} = 100 \times \frac{\mathrm{RMSE}_{\mathrm{baseline}} - \mathrm{RMSE}_{\mathrm{combined}}}{\mathrm{RMSE}_{\mathrm{baseline}}}. \tag{5}$$

Positive values denote lower prediction error after adding seismic features; negative values denote increased error. On identical test observations, R^2 and RMSE derive from the same squared prediction errors. Their changes therefore provide complementary descriptions of the same improvement, rather than independent evidence.

https://doi.org/10.5194/egusphere-2026-6435
Preprint. Discussion started: 26 October 2026
© Author(s) 2026. CC BY 4.0 License.

2.6 Model interpretation and data-availability analyses

2.6.1 SHAP-based feature interpretation

We use SHapley Additive exPlanations (SHAP) (Lundberg and Lee, 2017) to describe the contributions of individual predictors to fitted XGBoost predictions. SHAP values are calculated for the METEO + SEISMO and METEO + SOIL + SEISMO models. Mean absolute SHAP values summarize the magnitude of each contribution irrespective of its direction.

For the network-level comparison, SHAP values are evaluated on held-out test observations. Within each tree–station model, the mean absolute SHAP value of each predictor is expressed as a percentage of the sum across all predictors. For the network-level ranking of the METEO + SOIL + SEISMO models, equivalent seismic features are grouped independently of station identity. Contributions mapping to the same feature are summed within each tree–station model before their mean and 20th–80th percentile range are calculated across models containing that feature. Thus, station-specific bandpower estimates for the same frequency band appear as one predictor in the network-level ranking. Only the leading predictors are displayed, so their displayed percentages do not necessarily sum to 100%.

For the temporal analysis of the representative METEO + SOIL + SEISMO model, mean absolute SHAP values are calculated within successive 120-h blocks, with block sequences restarted in each growing season. Each block's feature contributions are normalized by the sum across all model predictors and expressed as percentages. Blocks with fewer than ten observations are omitted. The temporal heat map displays the eight predictors with the highest average blockwise importance and includes blocks from both training and held-out test observations. SHAP values describe contributions to model predictions; they do not establish causal effects.

2.6.2 Influence of seismic data availability

Source-level data coverage differs among stations and trees (Table S1; Fig. S1). For each tree–station pair, we additionally record the numbers of 15-min training and test samples retained for the METEO + SOIL + SEISMO model. These counts describe jointly available TWD and predictor observations, rather than raw dendrometer coverage, and are shown alongside absolute test performance and seismic gains in Fig. S6 of the Supplement. They provide descriptive context for differences between pairs and are not interpreted as evidence of a causal sample-size effect.

2.6.3 TWD variability and predictive gains

For each tree–station pair, TWD variability is quantified by the 90th–10th percentile range of observed TWD on matched held-out test observations pooled across the analysed growing seasons. Saved test predictions are checked against the exported sample counts, RMSE and R^2 before this diagnostic is calculated. The same variability measure is compared with seismic ΔR^2 and relative RMSE reduction for both nested baseline comparisons (Fig. S7 of the Supplement). The percentile range measures target variability, not persistent water deficit or drought severity. These comparisons are descriptive; combinations sharing trees or stations are not treated as independent replicates for pooled significance testing.

https://doi.org/10.5194/egusphere-2026-6435
Preprint. Discussion started: 26 October 2026
© Author(s) 2026. CC BY 4.0 License.

3 Results

3.1 Environmental conditions and tree water status

At the nearest DWD meteorological station (Lahr, station ID: 2812, 155 m a.s.l.), the mean summer (June–August) air temperature during the 1991–2020 reference period was 19.5 °C, and the mean summer precipitation sum was 247.2 mm (Deutscher Wetterdienst, 2023). All three summers were warmer than this reference, with mean air temperatures of 20.4, 20.6, and 22.8 °C in 2024, 2025, and 2026, respectively. Summer precipitation exceeded the reference mean in 2024 and 2025 (295.9 and 279.7 mm), but was substantially lower in 2026 (109.8 mm), making 2026 the warmest and driest of the three summers (Deutscher Wetterdienst, 2026).

The observations at ECOSENSE showed distinct conditions across the three growing seasons (Fig. 1D). Soil moisture at the measured profile varied seasonally, with additional intra-seasonal fluctuations. Compared with 2024 and 2025, summer 2026 showed a persistent decline in soil moisture, reaching the lowest observed levels at the end of August.

Absolute TWD was generally higher in Douglas fir than in European beech. Daily minimum TWD remained comparatively low in both species during 2024 and 2025, whereas elevated daily minima in 2026 indicated less complete overnight replenishment of stem water reserves. This pattern was particularly pronounced in Douglas fir.

These concurrent changes provide context for the latent-space and predictive analyses; the time series alone cannot establish how much of the TWD variation is attributable to soil moisture rather than other changing conditions.

3.2 Forest seismic dynamics occupy a structured network latent space

The station-wise spectral centroid frequencies form a structured PCA representation. PC1 explains 32.7% of the variance and PC2 explains 27.7%. Together, they account for 60.4%, while PC1–PC4 account for 99.6% of the variance after instantaneous network-mean subtraction, gap imputation and standardization (Fig. 2A). Observations form a continuous distribution in the PC1–PC2 plane rather than discrete clusters (Fig. 2B).

Wind speed varies systematically across this latent space. Higher wind speeds occur preferentially toward higher PC1 and PC2 scores, whereas low-wind observations occupy a broader region that extends toward lower scores (Fig. 2B). The observations overlap substantially across wind speeds, indicating continuous variation in the collective seismic response rather than distinct wind-dependent regimes.

The principal components combine seismic station responses in different ways. Stations C66 and C67 have positive PC1 loadings, whereas C69 and C6A have negative loadings; C68 has a pronounced positive loading on PC3 (Fig. 2C). The coordinates therefore represent contrasts across the station network rather than the behaviour of a single sensor.

Additional projections involving PC3 and PC4 reveal further organization by station contribution, wind speed, and growing season (Fig. S3 of the Supplement). The supplementary TWD projection illustrates Douglas fir Pm5. TWD also varies across these projections, but observations with different TWD values overlap extensively. Moreover, TWD ranges and data availability differ among growing seasons, so apparent seasonal and TWD-related patterns cannot be interpreted as independent effects.

https://doi.org/10.5194/egusphere-2026-6435
Preprint. Discussion started: 26 October 2026
© Author(s) 2026. CC BY 4.0 License.

Among the tested seismic descriptors, peak PSD frequency shows the clearest correspondence with the centroid-frequency PCA. After component matching, its scores correlate with the centroid-frequency scores at $r = 0.68$ for PC1 and $r = 0.33$–0.42 for PC2–PC4 (Fig. 2D). Variance, dominant spectral peak power, and the tested bandpowers show much weaker aligned score correspondence. The following latent-space analyses therefore use the centroid-frequency PCA.

3.3 Tree water status is associated with seismic latent-space occupancy

Tree water status is associated with differences in where observations occur within the continuous seismic latent space. For the representative Douglas fir Pm5, higher TWD values occur more frequently toward higher PC1 scores, whereas lower TWD values extend more broadly through the projection (Fig. 3A). The TWD ranges still overlap extensively across the latent space. The association is therefore expressed as a change in relative occupancy, not as a separate physiological cluster.

The conditional occupancy analysis shows how this association depends on wind conditions (Fig. 3B). Under low wind (< 2 m s^{-1}), observations extend toward lower PC1 and PC2 scores, with spatial variation in the probability of a dry TWD state within the occupied region. Moderate wind (2–5 m s^{-1}) spans a broader part of the projection and likewise shows variation in dry-state probability. Under high wind (> 5 m s^{-1}), observations are concentrated in a smaller region at higher PC1 and PC2 scores. Thus, wind changes the region sampled in seismic latent space, while TWD-defined dry-state probability varies within the wind-conditioned regions.

The time series places these TWD-defined states in their environmental context (Fig. 4A). For Pm5, the pooled thresholds classify observations as wet at TWD ≤ 0.04 µm and dry at TWD ≥ 46.20 µm. Wet observations predominate during much of 2024 and 2025 and in early 2026. Pm5 TWD then rises during summer 2026, producing an extended sequence of dry observations. Wet and dry observations nonetheless occur within overlapping ranges of PC1 scores and wind speeds; neither wind speed nor a single PCA coordinate uniquely identifies the TWD-defined state.

Within each wind class, the wet and dry PC1–PC2 distributions also overlap substantially (Fig. 4B). Their density contours and centroids indicate differences in relative occupancy, but the direction and magnitude of these differences depend on wind class. These comparisons support an association between Pm5 TWD and occupancy of the continuous, wind-dependent seismic latent space; they do not establish a separate seismic regime for wet or dry conditions.

3.4 Seismic predictors add information beyond environmental predictors

We tested whether seismic measurements improve quantitative TWD prediction beyond environmental predictors across 40 tree–station combinations. Adding seismic predictors to meteorology produces heterogeneous changes in held-out R^2, with positive gains for many pairs and negative changes for others (Fig. 5A). Including soil moisture improves absolute predictive performance for many trees, while the additional seismic contribution remains strongly pair-dependent (Fig. 5B; Fig. S5 of the Supplement). Pronounced soil-adjusted ΔR^2 gains occur for Pm1–C6A, several Fm1 combinations and Fm4 combinations. Most Pm2, Pm4, Pm5 and Fm2 combinations show much smaller changes on the R^2 scale.

Relative RMSE reduction provides an additional view of these changes (Fig. 5C). Some combinations with small soil-adjusted ΔR^2, including Pm2–C6A and several Pm5 combinations, nevertheless show appreciable relative reductions in pre-

https://doi.org/10.5194/egusphere-2026-6435
Preprint. Discussion started: 26 October 2026
© Author(s) 2026. CC BY 4.0 License.

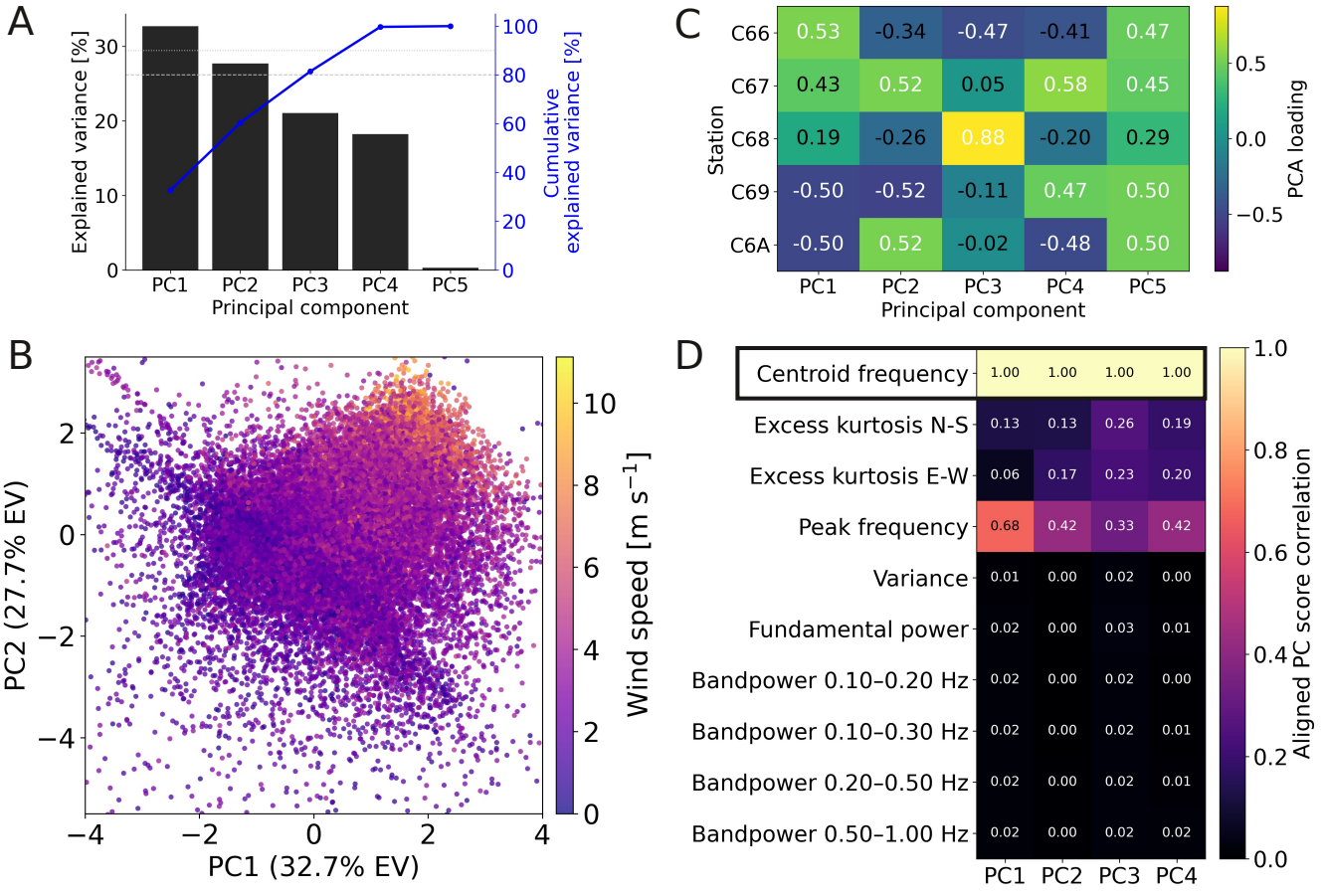


Figure 2. Organization of the forest seismic network in PCA space. **(A)** Explained variance of components derived from station-wise spectral centroid frequencies (black bars) and cumulative explained variance (blue line). **(B)** PC1–PC2 projection coloured by wind speed. **(C)** Station loadings for PC1–PC5. Analyses of latent-space occupancy use PC1–PC2; projections of PC3 and PC4 are shown in the Supporting Information. **(D)** Absolute correlations between centroid-frequency PC scores and scores from independently fitted PCA models using alternative seismic descriptors. Components were matched by their score time series before the correlations were calculated.

https://doi.org/10.5194/egusphere-2026-6435
Preprint. Discussion started: 26 October 2026
© Author(s) 2026. CC BY 4.0 License.

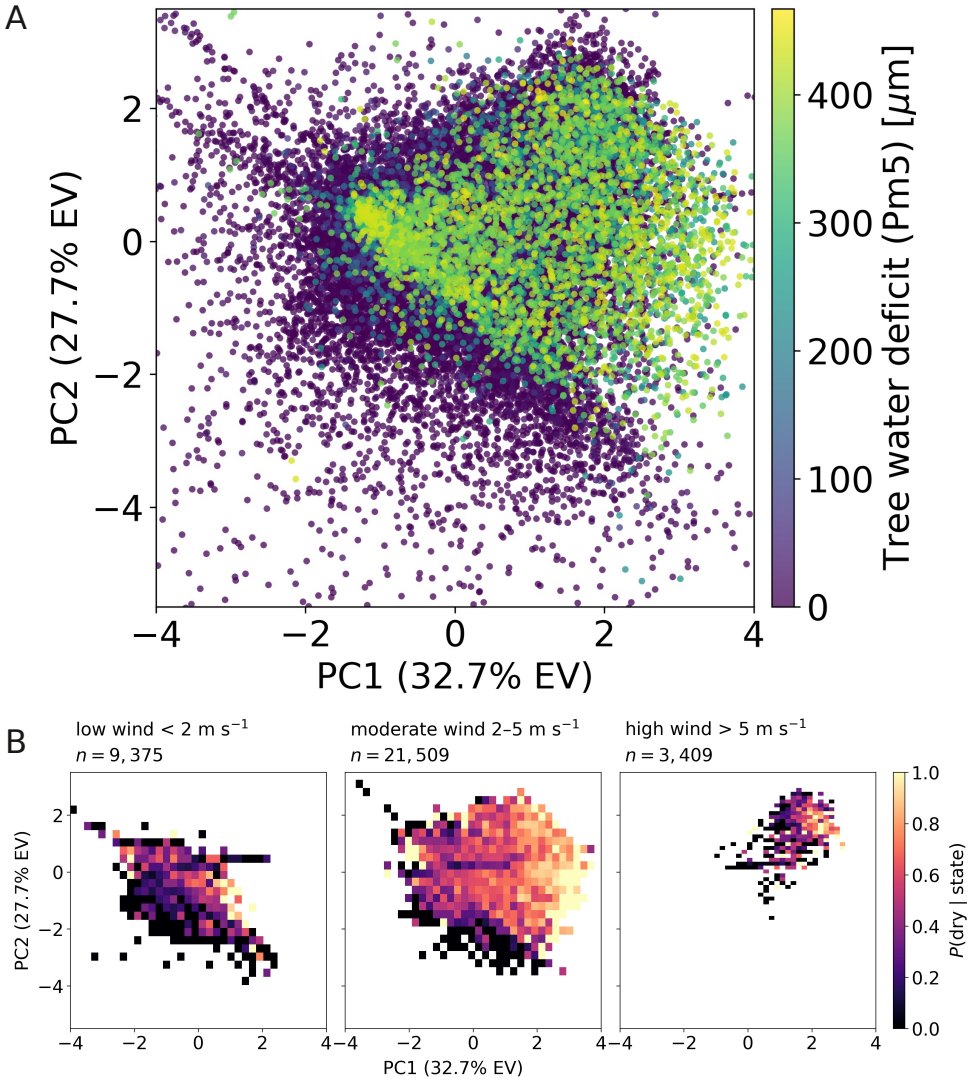


Figure 3. Tree water deficit (TWD) within the seismic latent space for the representative Douglas fir Pm5. **(A)** PC1–PC2 projection coloured by the corresponding Pm5 TWD. **(B)** Conditional probability of a dry TWD state, $P(\mathrm{dry} \mid \mathrm{state})$, in the PC1–PC2 projection under low (< 2 m s^{-1}), moderate (2–5 m s^{-1}), and high (> 5 m s^{-1}) wind speeds. Wet and dry states are defined by the lowest and highest 20%, respectively, of the available Pm5 TWD observations pooled across the three growing seasons. The value of n above each panel gives the number of observations in that wind class. Conditional probabilities use wet and dry observations only. Bins with fewer than 10 such observations are not coloured.

https://doi.org/10.5194/egusphere-2026-6435
Preprint. Discussion started: 26 October 2026
© Author(s) 2026. CC BY 4.0 License.

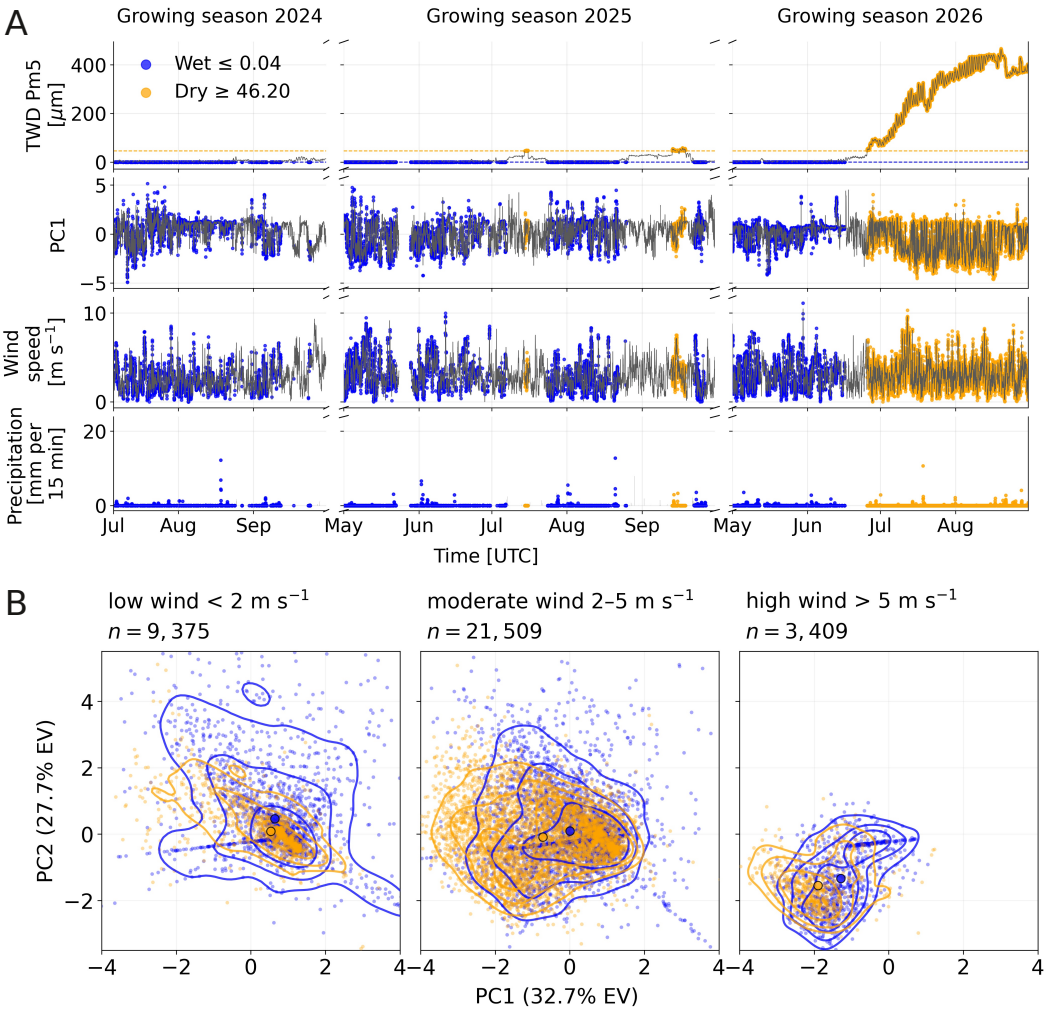


Figure 4. Temporal and wind-conditioned context of TWD-defined wet and dry observations for Douglas fir Pm5. **(A)** Time series during the 2024, 2025, and 2026 growing seasons showing, from top to bottom, Pm5 TWD, PC1 score, wind speed, and precipitation. Wet observations are shown in blue (TWD ≤ 0.04 µm) and dry observations in orange (TWD ≥ 46.20 µm); other available observations are shown in grey where applicable. The thresholds correspond to the lowest and highest 20% of available Pm5 TWD values pooled across the three growing seasons. Winter periods are omitted. **(B)** PC1–PC2 distributions of the TWD-defined wet and dry observations under low (< 2 m s^{-1}), moderate (2–5 m s^{-1}), and high (> 5 m s^{-1}) wind speeds. The value of n gives the number of observations in each wind class. Contours summarize the estimated density of each TWD state, and large outlined markers show their distribution centroids.

https://doi.org/10.5194/egusphere-2026-6435
Preprint. Discussion started: 26 October 2026
© Author(s) 2026. CC BY 4.0 License.

diction error. This occurs where the baseline already explains a high proportion of TWD variation. Pm1–C6A shows the largest displayed soil-adjusted relative RMSE reduction, at 26.4%, while some combinations exhibit increased error after adding seismic predictors. Across the 40 pairs, adding seismic predictors to METEO improves held-out R^2 in 27 cases, with a median ΔR^2 of 0.021 (range -0.045 to 0.149). Relative RMSE reductions have a median of 1.6% and range from -2.8% to 11.6%. After soil moisture adjustment, 34 pairs show positive gains, with a median ΔR^2 of 0.006 (range -0.012 to 0.166) and a median relative RMSE reduction of 2.2% (range -3.7% to 26.4%).

The four-model heatmaps in Fig. S5 of the Supplement show substantial differences in absolute test performance among trees. For example, METEO + SOIL achieves test R^2 of approximately 0.89–0.97 for Pm2, Pm4, Pm5 and Fm2, compared with approximately 0.12–0.21 for Fm1. High absolute R^2 does not necessarily imply a large incremental seismic gain. Figure S6 of the Supplement places these differences alongside the numbers of matched training and test samples. Fm1 has fewer usable observations than the other trees and lower absolute test R^2, but seismic gains remain positive across its five soil-adjusted comparisons.

The variability diagnostic shows no consistent monotonic increase in seismic gains with the held-out TWD percentile range (Fig. S7 of the Supplement). Fm1 shows positive soil-adjusted gains despite a relatively narrow TWD range, whereas Pm5 has the widest range and small soil-adjusted ΔR^2. Gains also vary among stations sampling similar TWD ranges for the same tree.

Across the soil-adjusted combined models, soil moisture has the largest mean relative absolute SHAP contribution among the displayed predictors (Fig. 5D). Air temperature at 2 m and bandpower at 0.20–0.50 Hz follow in the aggregated ranking. Other meteorological and seismic predictors have smaller average shares. Seismic features are summarized independently of station identity, with percentile ranges describing variation across the contributing tree–station models. This ranking describes the use of predictors by the fitted models and does not identify a universal seismic proxy or a causal mechanism for TWD.

3.5 Seasonal variation in predictions and predictor contributions

Douglas fir Pm1 and station C6A illustrate a pronounced seismic improvement after accounting for soil moisture (Fig. 6). On matched held-out test observations pooled across the three seasons, METEO achieves $R^2 = 0.32$ and RMSE $= 52.93$ µm. METEO + SEISMO achieves $R^2 = 0.47$ and RMSE $= 46.76$ µm. METEO + SOIL increases R^2 to 0.64 and reduces RMSE to 38.63 µm. Adding C6A seismic features to that baseline further increases R^2 to 0.80 and reduces RMSE to 28.42 µm, corresponding to an approximately 0.16 increase in R^2 and a 26.4% relative RMSE reduction.

METEO predictions capture some broad variation in TWD but show substantial deviations from the observations (Fig. 6A,F). Adding seismic predictors without soil moisture improves overall agreement, although substantial errors remain (Fig. 6B,F). The two soil-informed models provide closer agreement, with the full model achieving the lowest pooled test RMSE (Fig. 6C,D,F). No matched observations are available at the beginning of the 2026 growing season.

The relative contributions of the leading predictors change across and within growing seasons (Fig. 6E). In 2024, soil moisture contributes most strongly early in the observed period, while C6A bandpower at 0.50–1.00 Hz becomes more prominent later. Their relative contributions fluctuate during 2025. In the available part of 2026, soil moisture becomes increasingly dominant, while contributions from seismic bandpower and air temperature at 2 m remain smaller. These blockwise SHAP values

https://doi.org/10.5194/egusphere-2026-6435
Preprint. Discussion started: 26 October 2026
© Author(s) 2026. CC BY 4.0 License.

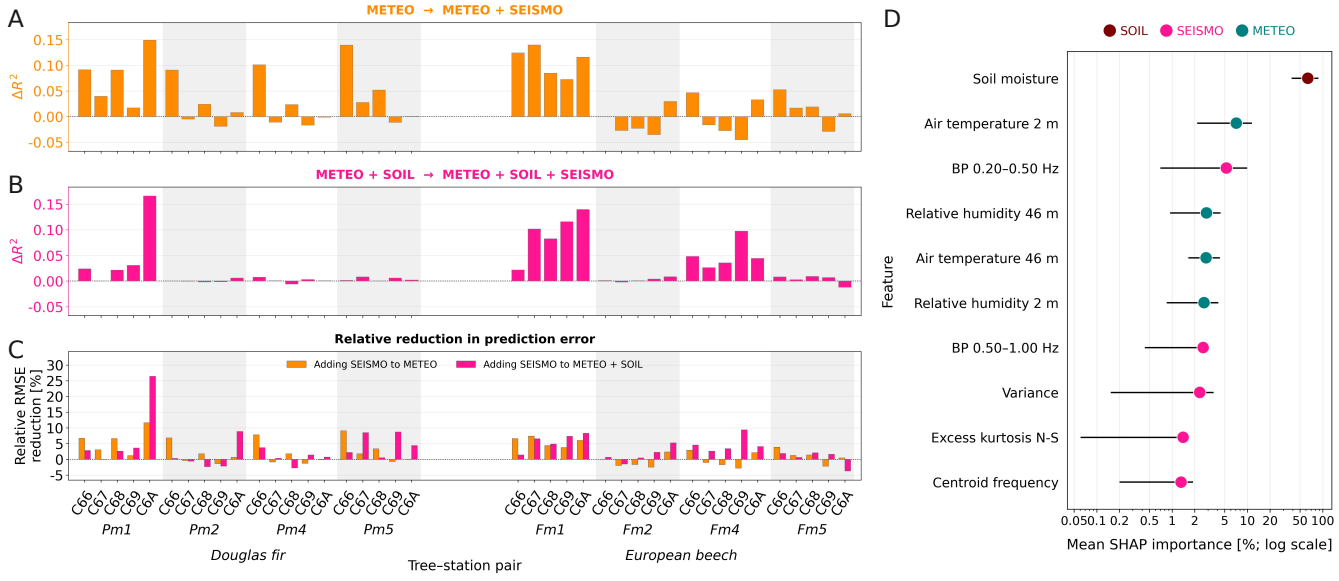


Figure 5. Added predictive value of seismic features across 40 tree–station combinations. **(A)** Change in held-out R^2 when seismic predictors are added to meteorology alone: METEO → METEO + SEISMO. **(B)** Change in held-out R^2 when seismic predictors are added to meteorology and soil moisture: METEO + SOIL → METEO + SOIL + SEISMO. **(C)** Relative reduction in held-out root mean squared error (RMSE) for the same comparisons, calculated as $100 \times (\mathrm{RMSE}_{\mathrm{baseline}} - \mathrm{RMSE}_{\mathrm{combined}})/\mathrm{RMSE}_{\mathrm{baseline}}$. Orange denotes the addition of seismic predictors to METEO, and pink their addition to METEO + SOIL. Positive values in (A)–(C) indicate improved predictive performance; negative values indicate deterioration. Each comparison uses matched held-out observations for the corresponding tree–station combination. Trees are grouped by species, with alternating shading distinguishing individual trees. **(D)** Leading predictors ranked by mean relative absolute SHAP contribution in the METEO + SOIL + SEISMO models. Mean absolute SHAP contributions are normalized to percentages within each tree–station model. Equivalent seismic features are grouped independently of station identity before averaging their contributions across models containing the respective feature. Colours distinguish meteorological, soil moisture, and seismic predictors. Horizontal lines show the 20th–80th percentile range of the corresponding per-model contributions. BP denotes bandpower, and N–S denotes the north–south component. Only the leading predictors are displayed.

https://doi.org/10.5194/egusphere-2026-6435
Preprint. Discussion started: 26 October 2026
© Author(s) 2026. CC BY 4.0 License.

describe how the fitted model uses its predictors; they do not identify the physical source of the seismic contribution or establish independent effects of correlated predictors.

4 Discussion

4.1 A network representation of wind-driven forest dynamics

Previous measurements at ECOSENSE established that wind-induced tree sway produces identifiable ground-motion signals and that seismic spectral features encode wind forcing (Umlauft et al., 2025). Whether these signals also carry information about tree water status has remained unresolved. Here, the latent-space and predictive analyses provide complementary evidence of associations between the wind-driven seismic response and dendrometer-derived TWD.

The five stations reveal a structured but continuous representation of ground motion across the forest plot. Their spectral centroid frequencies vary in coordinated ways, while station loadings indicate contrasts across the network rather than a signal from one dominant sensor. Wind speed strongly organizes the PC1–PC2 projection: higher-wind observations occur preferentially toward higher PC1 and PC2 scores, but observations at different wind speeds overlap. The network therefore captures a continuously varying, spatially heterogeneous response to wind rather than separate wind-dependent regimes.

The differing station contributions are consistent with the heterogeneous forest and measurement geometry. Trees vary in size, architecture, exposure, and mechanical properties, while each seismometer receives vibrations from multiple sources whose contributions depend on their location and coupling to the ground (Moore and Maguire, 2004; Jackson et al., 2019; Johnson et al., 2019; Umlauft et al., 2025). Neighbouring trees, canopy height, and canopy openness may further modify local wind exposure and the relative contributions of potential sources. The coordinated variation captured by PCA therefore coexists with differences among stations. The components describe patterns in the recorded network signals; they cannot be assigned to individual trees or specific physical modes without further source-localization evidence.

The centroid-frequency representation describes how spectral energy is distributed within the analysed frequency range. Frequency-based properties may be informative because tree motion depends on mass, stiffness, geometry, and damping as well as on the strength of wind forcing (Moore and Maguire, 2004; Jackson et al., 2019). Nevertheless, spectral centroid frequency is not a direct measurement of any one of these properties. Changes in source contributions or seismic propagation could also alter the recorded spectrum.

4.2 Tree water status is associated with latent-space occupancy

The occupancy analysis examines whether observations classified as wet or dry from individual-tree TWD occur with different relative frequencies across the PC1–PC2 projection. For Douglas fir Pm5, the conditional probability of a TWD-defined dry observation varies across this projection, including within wind-speed classes. Wet and dry observations nevertheless overlap substantially, and the direction and extent of their distributional differences depend on wind class. Neither state defines a separate seismic cluster or a unique PCA coordinate.

https://doi.org/10.5194/egusphere-2026-6435
Preprint. Discussion started: 26 October 2026
© Author(s) 2026. CC BY 4.0 License.

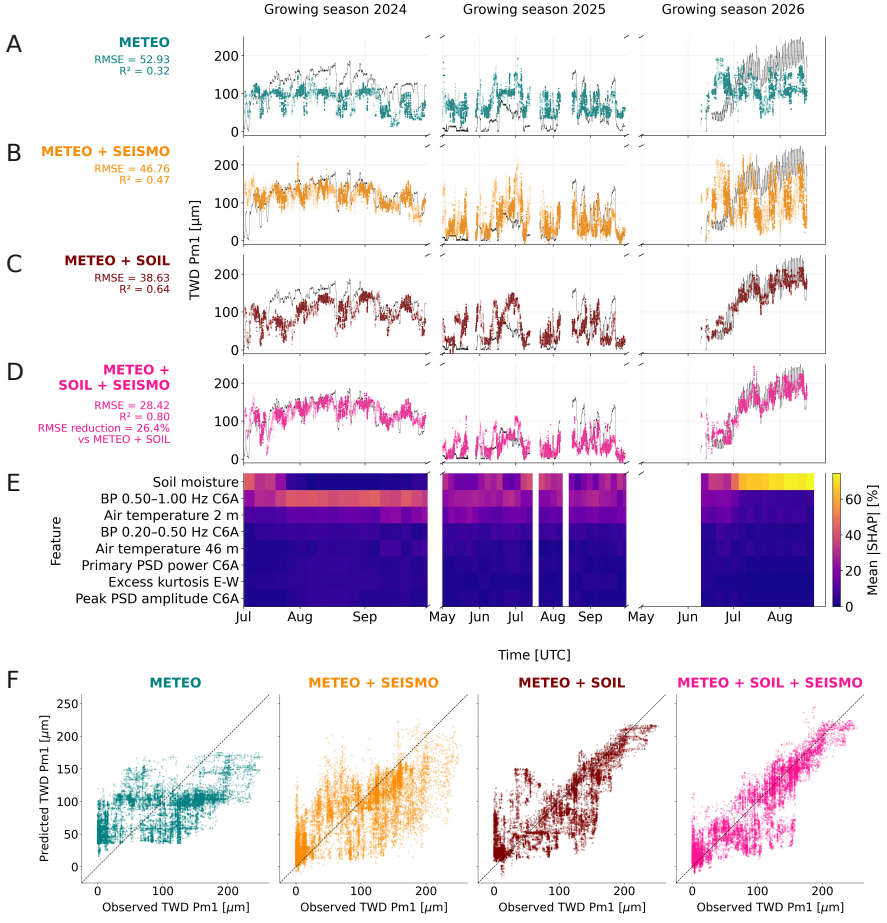


Figure 6. Temporal predictions and predictor contributions for Douglas fir Pm1 using seismic station C6A. **(A–D)** Observed tree water deficit (TWD; black) and predictions from METEO, METEO + SEISMO, METEO + SOIL, and METEO + SOIL + SEISMO, respectively, during the 2024, 2025, and 2026 growing seasons. Fainter points show training predictions and darker points show held-out test predictions. RMSE (in μm) and R^2 are calculated on matched held-out test observations pooled across the three seasons. Adding seismic predictors to METEO + SOIL reduces test RMSE by 26.4%. **(E)** Relative mean absolute SHAP contributions of the displayed leading predictors within successive 120-h blocks, calculated as percentages of the total mean absolute SHAP contribution across all predictors within each block for the METEO + SOIL + SEISMO model. Both training and test blocks are included in this descriptive analysis. BP denotes bandpower. **(F)** Observed versus predicted TWD on matched held-out test observations pooled across the three seasons for the four models, in the same order as panels A–D. Dashed lines indicate one-to-one agreement. Breaks in the time axes omit the intervening winter periods. Blank regions in the prediction panels indicate unavailable matched observations; blank regions in the SHAP panel indicate blocks without available SHAP estimates. Temporal data availability is shown in Fig. S1 of the Supporting Information.

https://doi.org/10.5194/egusphere-2026-6435
Preprint. Discussion started: 26 October 2026
© Author(s) 2026. CC BY 4.0 License.

This example demonstrates an association between Pm5 TWD and the collective seismic response. It does not establish how consistently comparable occupancy differences occur among the eight monitored trees. Quantifying that consistency would require a common measure of distributional separation, with uncertainty assessed while accounting for temporal dependence and unequal sample sizes. The network-wide predictive comparison provides a separate assessment of added seismic information, but does not quantify the prevalence of latent-space occupancy differences.

The mechanical coupling between tree sway and ground motion demonstrated by Umlauft et al. (2025) makes it plausible that changes in water status could alter the monitored seismic response. Changes in tree water content could affect mass distribution, tissue properties, and damping. Studies of tree sway have shown, for example, that canopy water intercepted during precipitation can change vibration periods (van Emmerik et al., 2017; Ciruzzi and Loheide II, 2021). TWD derived from stem diameter, however, is not a measurement of canopy water mass or any single mechanical property. The present association does not establish which aspect of the tree or its surroundings changes the recorded ground motion.

Forest structure also provides an important context for this interpretation. Neighbouring trees and differences in canopy height and openness may influence wind exposure, aerodynamic sheltering, and the mixture of tree-motion sources recorded by a station. These structural influences could modify the expression of water-status-related changes in the seismic response, but were not quantified here.

Wind stratification helps distinguish variation within broadly similar wind-speed conditions, but it cannot hold all relevant conditions constant. TWD covaries with season, temperature, humidity, precipitation, and soil water conditions (Brinkmann et al., 2016; Dumberger et al., 2025; Peters et al., 2025). Wind direction, gustiness, and differences in local exposure may also change which trees contribute most strongly to a station. Furthermore, soil conditions could influence tree anchorage, while changes in soil water content can alter seismic wave velocities (Shen et al., 2024) and potentially affect the propagation of vibrations from roots to seismometers. These pathways may occur together. The large overlap between wet and dry observations, and their unequal distribution among seasons, require caution when attributing the occupancy differences specifically to tree hydration.

We therefore interpret the latent-space result as evidence that TWD-related information may be embedded in a multivariate, wind-driven vibration field. It does not support a unique “dry-tree frequency” or a seismic classification of water status independent of environmental context.

4.3 Predictive value beyond measured environmental conditions

The predictive analysis extends the assessment to 40 tree–station combinations and shows that seismic information can improve TWD prediction beyond the measured environmental variables, although the benefits vary substantially (Fig. 5). Soil moisture provides a large improvement in absolute predictive performance for many trees. Additional seismic gains on the R^2 scale are often small where the soil-informed baseline already performs well, while larger gains remain for Pm1–C6A and several beech combinations. Negative gains for some pairs show that additional seismic predictors do not invariably improve held-out prediction.

https://doi.org/10.5194/egusphere-2026-6435
Preprint. Discussion started: 26 October 2026
© Author(s) 2026. CC BY 4.0 License.

Relative RMSE reduction is useful for interpreting small ΔR^2 near the baseline performance ceiling. Some Pm2 and Pm5 combinations show reductions in error despite small changes in R^2 (Fig. 5C). These two metrics describe the same underlying squared errors on matched observations; their agreement is not independent confirmation. Positive changes alone also do not establish that an improvement is statistically distinguishable from sampling or model-fitting variability.

Pm1–C6A illustrates a substantial soil-adjusted improvement: held-out R^2 increases from 0.64 to 0.80 and RMSE decreases from 38.63 to 28.42 μm, a reduction of 26.4% (Fig. 6). This is the largest soil-adjusted relative reduction displayed in the network summary, rather than a typical outcome across all combinations.

The predictive gains do not identify their physical origin. Seismic features may encode aspects of wind excitation and local exposure that are incompletely measured at the tower, as well as vegetation motion, source–ground coupling, or changes in propagation. Environmental predictors account for some of the shared variation; they cannot separate these possible pathways. Thus, improved TWD prediction does not by itself demonstrate that a seismometer directly senses a change in tree hydration.

The variation among tree–station combinations is consistent with the measurement geometry. A dendrometer describes one stem, whereas a seismometer records ground motion generated by multiple surrounding sources. The seismic contribution to the prediction of a given tree's TWD may therefore depend on source–receiver geometry, tree dimensions, neighbouring vegetation, canopy structure, local wind exposure, and the degree to which its water status covaries with that of other trees. Differences in data availability, the distribution of environmental conditions within available blocks, and measurement quality may also contribute to the observed variation in gains. The matched-availability summary (Fig. S6 of the Supplement) provides context for these differences, but does not isolate an effect of sample size. In particular, Fm1 combines reduced coverage and low absolute predictive performance with positive soil-adjusted seismic gains. Its available observations also cover a different subset of seasons and environmental conditions.

The variability analysis further shows that greater TWD variation does not consistently imply greater incremental seismic benefit (Fig. S7 of the Supplement). The contrast between Fm1 and Pm5 illustrates this distinction. However, the percentile range measures the spread of the available target values, not drought severity, and the pairs share trees and stations. These diagnostics therefore help interpret heterogeneity without establishing independent or causal effects of availability or TWD variability.

Across the soil-adjusted models, soil moisture has the largest mean relative absolute SHAP contribution among the displayed predictors, while seismic bandpower features contribute smaller shares that vary among combinations. The temporal analysis for Pm1–C6A further illustrates how predictor contributions can change within a fitted model. Soil moisture is influential early in the observed part of 2024, whereas 0.50–1.00 Hz bandpower becomes more prominent later; soil moisture increasingly dominates during the available part of 2026. These variations are compatible with context-dependent predictive relationships, but their joint physical interpretation remains open.

In the temporal analysis, SHAP contributions are expressed relative to all model predictors within each block, so a change in one feature's share need not imply a corresponding change in the strength of its physical relationship with TWD. Correlated soil, meteorological, and seismic variables can also share predictive information. The selected hyperparameters are summarized in Fig. S4 of the Supporting Information; their frequencies describe fitting choices rather than the robustness of

https://doi.org/10.5194/egusphere-2026-6435
Preprint. Discussion started: 26 October 2026
© Author(s) 2026. CC BY 4.0 License.

a proposed mechanism. Together, the predictive results favour a context-dependent combination of seismic descriptors over a single universal seismic proxy for TWD.

4.4 Potential for forest monitoring

Direct physiological measurements remain essential for interpreting tree water status. Dendrometers, sap-flow sensors, and measurements of leaf water potential or leaf gas exchange provide information tied to individual plants, but continuous coverage of many trees requires substantial installation and maintenance. Seismometers offer a different observation: they can record continuously without being attached to tree stems and can sample vibrations generated by several surrounding sources (Johnson et al., 2019; Umlauft et al., 2025). Their value lies in measuring a mechanical response that complements direct physiological and meteorological observations.

The combination of observation types is particularly useful because each addresses a different part of the system. Meteorological measurements characterize external forcing; soil moisture measurements characterize local subsurface conditions; dendrometers provide tree-specific responses; and the seismic network records ground vibrations produced by the coupled vegetation–ground system. The present results show that seismic measurements can improve TWD prediction after environmental variables are supplied to the model, although the size of the improvement varies substantially. Seismic monitoring therefore requires calibration against direct observations and careful consideration of sensor placement and forest structure.

Our analysis applies a stringent criterion for assessing seismic information: seismic features must improve held-out TWD prediction after meteorological and soil moisture measurements are already available to the model. Operational monitoring need not require this incremental benefit. Seismic features could be useful if they predict TWD reliably, including through information shared with environmental conditions. The additional predictive value observed for many tree–station combinations therefore strengthens the case for their monitoring potential. However, the performance of models using seismic predictors alone, or together with soil moisture but without meteorological inputs, remains to be evaluated.

One potential application is to characterize the seismic response expected under measured environmental conditions and examine sustained departures from it. The continuous latent space provides a way to describe such changes without assigning fixed stress thresholds to individual seismic features. This study has not tested whether those departures reliably indicate physiological change. That application requires validation against direct tree measurements across different environmental conditions and sites.

4.5 Limitations and future directions

The study covers one heterogeneous forest plot, five seismic stations, eight dendrometer-equipped trees, and three growing seasons. The observations span different meteorological, tree- and soil-water conditions, including a pronounced increase in Douglas-fir TWD in 2026, but do not establish that the relationships transfer to other forests. The 120-h blocked evaluation tests prediction on unseen multi-day periods within the observed seasons. It does not test transfer to an entirely withheld season or site. Adjacent training and test blocks can also retain similarity in slowly varying environmental conditions. Accordingly, the reported performance should be understood as within-site, within-season blocked performance.

https://doi.org/10.5194/egusphere-2026-6435
Preprint. Discussion started: 26 October 2026
© Author(s) 2026. CC BY 4.0 License.

The 40 tree–station combinations share trees, stations, and environmental conditions and therefore do not constitute 40 independent biological replicates. Counts of positive gains describe the evaluated combinations, while broader inference requires replication across independent trees, plots, and sites. Likewise, the illustrated Pm5 occupancy differences should not be assumed to characterize all monitored trees. A systematic comparison across trees, using common effect-size measures and uncertainty estimates, would help establish the consistency of these patterns.

The spatial sensitivity of each seismic station is not known. Multiple trees can contribute to one ground-motion record, and the monitored dendrometer trees are only a subset of potential sources. Horizontal distance between a monitored tree and a station therefore provides only a partial description of their relationship. Tree motion, ground coupling, forest structure, and contributions from other trees also affect the recorded signal. Future analyses should explicitly consider neighbouring-tree dimensions and positions, canopy height, canopy openness, and local wind exposure.

Soil moisture was represented by the median across four depths at one profile, providing a local environmental predictor without resolving conditions throughout the rooting zones of all monitored trees. Differences in substrate and propagation paths may also affect seismic features. Future measurements combining a denser seismic array, simultaneous tree acceleration, local wind observations, structural information, and spatially distributed soil measurements could help separate source motion from ground transmission and constrain the area represented by each station.

Finally, the observational design cannot isolate the causal effect of tree water status on seismic dynamics. Wind, seasonal vegetation changes, tree physiology, and soil conditions evolve together. Frequency-based features remain sensitive to source mixtures and propagation, even when they are less dependent on absolute signal amplitude. A controlled drying and rewetting experiment, with simultaneous measurements of tree motion and ground motion, would provide a more direct test of how changes in hydration alter the seismic response. Repeating the analysis across forests with different structure, species, and soils would then show which relationships are transferable.

5 Conclusions

Building on evidence that wind-driven tree motion can be recorded in ground vibrations, this study shows that a five-station seismic network captures a continuous, spatially structured response organized strongly by wind. Tree water deficit is associated with subtler differences in latent-space occupancy, although wet and dry observations overlap rather than forming separate seismic regimes.

Seismic features improve held-out tree water deficit prediction beyond meteorological predictors, with substantial improvements for particular tree–station combinations even after accounting for soil moisture. The heterogeneous gains indicate that the predictive value of seismic observations depends on the monitored tree and station; the conditions under which they provide the greatest benefit remain to be established. These results demonstrate that forest ground vibrations can contribute information about tree water deficit beyond the measured environmental variables, while leaving the physical origin of that contribution unresolved.

https://doi.org/10.5194/egusphere-2026-6435
Preprint. Discussion started: 26 October 2026
© Author(s) 2026. CC BY 4.0 License.

With validation across sites and conditions, seismic networks could complement direct physiological measurements by tracking changes in forest mechanical response relative to measured environmental conditions. Direct tree measurements remain essential for interpreting those changes.

Code and data availability. The compiled 15-minute dataset, analysis code, reference model results and software environment specifications are publicly available on Zenodo at https://zenodo.org/records/23415966. The archive includes documentation for reproducing the analyses from the compiled dataset and notebooks documenting raw data processing.

Raw observations are not included because of their large volume and because some data remain under embargo. They are available upon request from the corresponding author (josefine.umlauft@uni-leipzig.de). The complete seismic raw dataset is scheduled for public release through GEOFON, GFZ Potsdam, by the end of 2026.

Author contributions. Josefine Umlauft, Karin Mora and Teja Kattenborn conceptualized the study. Josefine Umlauft and Kilian Gerberding conducted the seismic fieldwork. Stefanie Dumberger, Simon Haberstroh and Christiane Werner provided the dendrometer observations used to derive tree water deficit. Markus Sulzer provided the meteorological observations. Lea Dedden and Markus Weiler provided the soil moisture observations.

Josefine Umlauft developed and implemented the analysis workflow, including data integration and preprocessing, seismic feature extraction, principal component analysis, predictive modelling, model interpretation and visualization, and prepared the reproducibility archive. Josefine Umlauft wrote the initial manuscript draft. All authors contributed to the interpretation of the results and critically reviewed and revised the manuscript.

Competing interests. The authors declare that they have no competing interests.

Acknowledgements. The authors gratefully acknowledge financial support from the Federal Ministry of Research, Technology and Space of Germany and the Saxon State Ministry for Science, Culture and Tourism through the Center of Excellence for AI Research "Center for Scalable Data Analytics and Artificial Intelligence Dresden/Leipzig" (ScaDS.AI), project identification number: ScaDS.AI. We also acknowledge funding from the German Research Foundation (DFG) through the Collaborative Research Centre CRC 1537 ECOSENSE.

We thank the Geophysical Instrument Pool Potsdam (GIPP), particularly Dr. Christian Haberland, for providing instrumentation.

Karin Mora acknowledges funding from the Saxon State Ministry for Science, Culture and Tourism (SMWK; 3-7304/35/6-2021/48880) and the ESA AI4Science project "DeepFeatures" (2024–2026).

We thank the iDiv Research Platform ARBOfun—Research Arboretum Großpösna for supporting preliminary tests and contributing to the conceptual development of the study during preparation of the CRC proposal BBCe (Biodiversity Buffers Climate Extremes).

https://doi.org/10.5194/egusphere-2026-6435
Preprint. Discussion started: 26 October 2026
© Author(s) 2026. CC BY 4.0 License.

References

Allen, C. D., Breshears, D. D., and McDowell, N. G.: On underestimation of global vulnerability to tree mortality and forest die-off from hotter drought in the Anthropocene, Ecosphere, 6, 1–55, https://doi.org/10.1890/ES15-00203.1, 2015.

Brinkmann, N., Eugster, W., Zweifel, R., Buchmann, N., and Kahmen, A.: Temperate tree species show identical response in tree water deficit but different sensitivities in sap flow to summer soil drying, Tree Physiology, 36, 1508–1519, https://doi.org/10.1093/treephys/tpw062, 2016.

Chen, T. and Guestrin, C.: XGBoost: A Scalable Tree Boosting System, in: Proceedings of the 22nd ACM SIGKDD International Conference on Knowledge Discovery and Data Mining, KDD '16, pp. 785–794, Association for Computing Machinery, New York, NY, USA, ISBN 978-1-4503-4232-2, https://doi.org/10.1145/2939672.2939785, 2016.

Ciruzzi, D. M. and Loheide II, S. P.: Monitoring Tree Sway as an Indicator of Water Stress, Geophysical Research Letters, 46, 12 021–12 029, https://doi.org/https://doi.org/10.1029/2019GL084122, 2019.

Ciruzzi, D. M. and Loheide II, S. P.: Monitoring Tree Sway as an Indicator of Interception Dynamics Before, During, and Following a Storm, Geophysical Research Letters, 48, e2021GL094 980, https://doi.org/10.1029/2021GL094980, 2021.

Deutscher Wetterdienst: Vieljährige Mittelwerte, https://www.dwd.de/DE/leistungen/klimadatendeutschland/vielj_mittelwerte.html, accessed 7 September 2026, 2023.

Deutscher Wetterdienst: Climate Data Center (CDC) Observations Germany, Climate, Daily Values (KL), Lahr Station (02812), https://opendata.dwd.de/climate_environment/CDC/observations_germany/climate/annual/kl/historical/, accessed 20 August 2026, 2026.

Dietrich, L., Zweifel, R., and Kahmen, A.: Daily stem diameter variations can predict the canopy water status of mature temperate trees, Tree Physiology, 38, 941–952, https://doi.org/10.1093/treephys/tpy023, 2018.

Donfack, L. S., Mund, M., Koebsch, F., Schall, P., Heidenreich, M. G., Seidel, D., and Ammer, C.: Linking sap flow and tree water deficit in an unmanaged, mixed beech forest during the summer drought 2022, Plant Biology, 28, 747–761, https://doi.org/https://doi.org/10.1111/plb.13754, 2026.

Dorigo, W., Xaver, A., Vreugdenhil, M., Gruber, A., Hegyiová, A., Sanchis-Dufau, A., Zamojski, D., Cordes, C., Wagner, W., and Drusch, M.: Global Automated Quality Control of In Situ Soil Moisture Data from the International Soil Moisture Network, Vadose Zone Journal, 12, vzj2012.0097, https://doi.org/https://doi.org/10.2136/vzj2012.0097, 2013.

Dumberger, S., Kinzinger, L., Weiler, M., Werner, C., and Haberstroh, S.: Dynamic Shifts in Radial Sap Flow of Two Temperate Tree Species in Response to the Dry Summer 2022, Ecohydrology, 18, e70 054, https://doi.org/https://doi.org/10.1002/eco.70054, e70054 ECO-25-0036.R1, 2025.

Dumberger, S., Frey, Y., Stock, C., Wehlings-Schmitz, S., Wagner, D., Kühnhammer, K., Dedden, L., Weiler, M., Sulzer, M., Christen, A., Kreuzwieser, J., Wallrabe, U., Werner, C., and Haberstroh, S.: Seasonal dynamics and sun/shade heterogeneity of leaf gas exchange and VOC emissions inside a tall temperate forest canopy, Tree Physiology, p. tpag111, https://doi.org/10.1093/treephys/tpag111, 2026.

Gessler, A., Grünzweig, J. M., Bigio, L., Hartmann, H., McDowell, N., Krumm, F., Bose, A. K., Rigling, A., Bugmann, H., Vitali, V., Schneider, P., Lever, J. J., Schweier, J., Kempel, A., Zimmermann, N. E., Brun, P., Bauhus, J., Wilhelm, M., and Bottero, A.: Shaping future forests: how can ecophysiology support climate-smart forest management?, New Phytologist, 250, 2778–2813, https://doi.org/10.1111/nph.71007, 2026.

https://doi.org/10.5194/egusphere-2026-6435
Preprint. Discussion started: 26 October 2026
© Author(s) 2026. CC BY 4.0 License.

Haberstroh, S., Scarpa, F., Seeger, S., Christen, A., and Werner, C.: Continuous Stem Water Potential Measurements of a Diffuse-Porous Tree Species Offer New Insights Into Tree Water Relations, Ecohydrology, 18, e2761, https://doi.org/https://doi.org/10.1002/eco.2761, e2761 ECO-24-0173.R1, 2025.

Hackmann, C. A., Sennhenn-Reulen, H., Mund, M., and Ammer, C.: Local neighborhood affects stem rehydration under drought: evidence from mixtures of European beech with two different conifers, Tree Physiology, 44, tpae114, https://doi.org/10.1093/treephys/tpae114, 2024.

Jackson, T., Shenkin, A., Moore, J. R., Bunce, A., van Emmerik, T., Kane, B., Burcham, D., James, K., Selker, J., Calders, K., Origo, N., Disney, M., Burt, A., Wilkes, P., Raumonen, P., de Tanago Menaca, J. G., Lau, A., Herold, M., Goodman, R. C., Fourcaud, T., and Malhi, Y.: An architectural understanding of natural sway frequencies in trees, Journal of The Royal Society Interface, 16, 20190 116, https://doi.org/10.1098/rsif.2019.0116, 2019.

Johnson, C. W., Meng, H., Vernon, F., and Ben-Zion, Y.: Characteristics of Ground Motion Generated by Wind Interaction With Trees, Structures, and Other Surface Obstacles, Journal of Geophysical Research: Solid Earth, 124, https://doi.org/10.1029/2018JB017151, 2019.

Knüsel, S., Peters, R. L., Haeni, M., Wilhelm, M., and Zweifel, R.: Processing and Extraction of Seasonal Tree Physiological Parameters from Stem Radius Time Series, Forests, 12, https://doi.org/10.3390/f12060765, 2021.

Lundberg, S. M. and Lee, S.-I.: A unified approach to interpreting model predictions, in: Advances in Neural Information Processing Systems, vol. 30, pp. 4765–4774, Curran Associates, Inc., 2017.

Magh, R.-K., Paligi, S. S., Papastefanou, P., Klosterhalfen, A., Ammer, C., Beyer, M., Dubbert, M., Haberstroh, S., Rohde, C., Werner, C., and Hildebrandt, A.: Continuous Stem Water Potential Measurements With Microtensiometry Reveal Species Identity and Soil Matric Potential Control of Stem Water Potential in Temperate Forests, Ecohydrology, 19, e70 197, https://doi.org/10.1002/eco.70197, 2026.

Mahecha, M. D., Bastos, A., Bohn, F., Eisenhauer, N., Feilhauer, H., Hickler, T., Kalesse-Los, H., Migliavacca, M., Otto, F. E. L., Peng, J., Tegen, I., Weigelt, A., Wendisch, M., Wirth, C., Al-Halbouni, D., Deneke, H. M., Doktor, D., Dunker, S., Ehrlich, A., Foth, A., Garcia-Garcia, A., Guerra, C. A., Guimaraes-Steinicke, C., Hartmann, H., Henning, S., Herrmann, H., Ji, C., Kattenborn, T., Kolleck, N., Kretschmer, M., Kühn, I., Luttkus, M. L., Maahn, M., Mönks, M., Mora, K., Pöhlker, M., Reichstein, M., Rüger, N., Sánchez-Parra, B., Schäfer, M., Sippel, S., Tesche, M., Wehner, B., Wieneke, S., Winkler, A., Wolf, S., Zaehle, S., Zscheischler, J., and Quaas, J.: Biodiversity and climate extremes: known interactions and research gaps, Earth's Future, 12, e2023EF003 963, https://doi.org/https://doi.org/10.1029/2023EF003963, 2024.

Moore, J. R. and Maguire, D. A.: Natural sway frequencies and damping ratios of trees: concepts, review and synthesis of previous studies, Trees, 18, 195–203, 2004.

Peters, R. L., Basler, D., Zweifel, R., Steger, D. N., Zhorzel, T., Zahnd, C., Hoch, G., and Kahmen, A.: Normalized tree water deficit: an automated dendrometer signal to quantify drought stress in trees, New Phytologist, 247, 1186–1198, https://doi.org/https://doi.org/10.1111/nph.70266, 2025.

Shen, Z., Yang, Y., Fu, X., Adams, K. H., Biondi, E., and Zhan, Z.: Fiber-optic seismic sensing of vadose zone soil moisture dynamics, Nature Communications, 15, 6432, https://doi.org/10.1038/s41467-024-50690-6, 2024.

Tesch, J., Kühnhammer, K., Wagner, D., Christen, A., Dormann, C., Frey, J., Grote, R., Kattenborn, T., Sulzer, M., Wallrabe, U., Weiler, M., Werner, C., Baghbani, S., Brzozon, J., Comella, L. M., Dedden, L., Dumberger, S., Frey, Y., Gassilloud, M., Gerach, T., Göritz, A., Haberstroh, S., Klüppel, J., Kremer, L., Kreuzwieser, J., Lee, H., Maack, J., Müller, J., Prucker, O., Rajak, S. K., Rühe, J., Rupitsch, S. J., Schack-Kirchner, H., Scharinger, C., Shinde, U., Steinmann, T., Stock, C., and Strack, J.: The ECOSENSE forest: A

https://doi.org/10.5194/egusphere-2026-6435
Preprint. Discussion started: 26 October 2026
© Author(s) 2026. CC BY 4.0 License.



distributed sensor and data management system for real-time monitoring of ecosystem processes and stresses, EGUsphere, 2025, 1–29, https://doi.org/10.5194/egusphere-2025-4979, 2025.

Tesch, J., Kühnhammer, K., Wagner, D., Christen, A., Dormann, C., Frey, J., Grote, R., Kattenborn, T., Sulzer, M., Wallrabe, U., Weiler, M., Werner, C., Baghbani, S., Brzozon, J., Comella, L. M., Dedden, L., Dumberger, S., Frey, Y., Gassilloud, M., Gerach, T., Göritz, A., Haberstroh, S., Klüppel, J., Kremer, L., Kreuzwieser, J., Lee, H., Maack, J., Müller, J., Prucker, O., Rajak, S. K., Rühe, J., Rupitsch, S. J., Schack-Kirchner, H., Scharinger, C., Shinde, U., Steinmann, T., Stock, C., and Strack, J.: The ECOSENSE forest: a distributed sensor and data management system for real-time monitoring of ecosystem processes and stresses, Geoscientific Instrumentation, Methods and Data Systems, 15, 253–272, https://doi.org/10.5194/gi-15-253-2026, 2026.

Topp, G. C., Davis, J. L., and Annan, A. P.: Electromagnetic determination of soil water content: Measurements in coaxial transmission lines, Water Resources Research, 16, 574–582, https://doi.org/https://doi.org/10.1029/WR016i003p00574, 1980.

Umlauft, J., Mora, K., Limberger, F., Gerberding, K., Wirth, C., Werner, C., and Kattenborn, T.: The seismic fingerprint of wind-induced tree sway, Methods in Ecology and Evolution, 16, 2886–2900, https://doi.org/10.1111/2041-210X.70173, 2025.

van Emmerik, T., SteeleDunne, S., Hut, R., Gentine, P., Guerin, M., Oliveira, R. S., Wagner, J., Selker, J., and van de Giesen, N.: Measuring Tree Properties and Responses Using Low-Cost Accelerometers, Sensors, 17, 1098, https://doi.org/10.3390/s17051098, 2017.

Welch, P.: The use of fast Fourier transform for the estimation of power spectra: A method based on time averaging over short, modified periodograms, IEEE Transactions on Audio and Electroacoustics, 15, 70–73, https://doi.org/10.1109/TAU.1967.1161901, 1967.

Werner, C., Wallrabe, U., Christen, A., Comella, L., Dormann, C., Göritz, A., Grote, R., Haberstroh, S., Jouda, M., Kiese, R., et al.: ECOSENSE-Multi-scale quantification and modelling of spatio-temporal dynamics of ecosystem processes by smart autonomous sensor networks, Research Ideas and Outcomes, 10, e129 357, 2024.

Werner, C., Bahn, M., Grams, T. E. E., Grossiord, C., Haberstroh, S., Lenczner, G., Tuia, D., and Vallicrosa, H.: Impact of emerging compound droughts on forests: a water supply and demand perspective, Plant Biology, https://doi.org/10.1111/plb.70080, 2025.

Ziegler, Y., Grote, R., Alongi, F., Knüver, T., and Ruehr, N. K.: Capturing drought stress signals: the potential of dendrometers for monitoring tree water status, Tree Physiology, 44, tpae140, https://doi.org/10.1093/treephys/tpae140, 2024.

Zweifel, R., Zimmermann, L., and Newbery, D. M.: Modeling tree water deficit from microclimate: an approach to quantifying drought stress, Tree Physiology, 25, 147–156, https://doi.org/10.1093/treephys/25.2.147, 2005.

Zweifel, R., Haeni, M., Buchmann, N., and Eugster, W.: Are trees able to grow in periods of stem shrinkage?, New Phytologist, 211, 839–849, https://doi.org/https://doi.org/10.1111/nph.13995, 2016.

Zweifel, R., Etzold, S., Sterck, F., Gessler, A., Anfodillo, T., Mencuccini, M., von Arx, G., Lazzarin, M., Haeni, M., Feichtinger, L., Meusburger, K., Knuesel, S., Walthert, L., Salmon, Y., Bose, A. K., Schoenbeck, L., Hug, C., De Girardi, N., Giuggiola, A., Schaub, M., and Rigling, A.: Determinants of legacy effects in pine trees – implications from an irrigation-stop experiment, New Phytologist, 227, 1081–1096, https://doi.org/10.1111/nph.16582, 2020.